21st Australasian Fluid Mechanics Conference
Adelaide, Australia
10-13 December 2018

CFD Simulations of a Newly Developed Floating Offshore Wind Turbine Platform using OpenFOAM

H. Sarlak, A. Pegalajar-Jurado and H. Bredmose

Fluid Mechanics Section, Department of Wind Energy

Technical University of Denmark, 2800 Kgs. Lyngby, Denmark

Abstract

The development of floating offshore wind farms relies on the efficient design of floating wind turbine platforms. In this paper, we present validations of two-phase flow simulations of the newly developed LIFES50+ OO-Star Wind Floater Semi 10 MW (OO-Star floater) (W. Yu, K. Müller, 2018) using the open source toolbox OpenFOAM. Free decay simulations of the platform are performed and cross-validated against a FAST model (Pegalajar-Jurado, Bredmose, *et al.*, 2018; Pegalajar-Jurado, Madsen, *et al.*, 2018). Further, the forcing on the fixed platform and the loads on the free and moored platform in regular waves are analysed and generally, a very good agreement is seen for the natural frequency, magnitude of damping and trend of increased damping for larger motion amplitude.

Introduction

The development of offshore wind farms at intermediate and large depths relies on the efficient design of floating platforms. Model-scale experimental studies have been performed in recent years to investigate the dynamic responses of various concepts (Martin *et al.*, 2014; Bredmose *et al.*, 2015, 2017; Pegalajar-Jurado *et al.*, 2016) Experimental investigations are, however, limited in accuracy due to their inability to achieve aerodynamic Reynolds similarity at the same time as Froude scaling is applied. Alternatively, full-scale numerical simulations have been applied to overcome such limitations (Alexander J. Dunbar, Craven and Paterson, 2015; Bruinsma, 2016). While the dynamic response of floaters in wind and waves is often well predicted by the aero-hydro-elastic models such as FAST, the forcing from strongly nonlinear waves, viscous damping effects and green-water events require higher fidelity modelling such as fully coupled computational fluid dynamics (CFD) simulations.

Numerous studies have been performed in recent years to investigate the interaction of waves with fixed and floating bodies (Sarlak, Seif and Abbaspour, 2010; Paulsen *et al.*, 2014). Benitz *et al.*, (2014) performed CFD simulations for the Offshore Code Comparison Collaboration Continuation (OC4) project using OpenFOAM and compared results against engineering models. They found discrepancies in load predictions and related them to a variety of factors, including shadowing effects, treatment of the interaction between individual floater members and the selection or prediction of drag coefficients. Recently, two 10MW reference floaters have been designed and published by the H2020 LIFES50+ project (www.lifes50plus.eu), which focuses on the next generation of substructures for floating offshore wind turbines. This paper presents CFD simulations of the OO-Star Wind Floater Semi 10 MW, hereafter called OO-Star floater, and comparison against a state-of-the-art model.

Simulation setup

The CFD simulations are performed using the open source solver openFOAM. The two-phase incompressible Navier–Stokes solver interDyMFoam is used, in which a volume of fluid approach is employed for tracking the free surface, and mesh motion and deformation capability is included. The fluid solver is combined with waves2Foam library to support wave generation and absorption, and the solver uses PIMPLE algorithm for pressure-velocity coupling. A non-conformal grid is generated and refined by importing the geometry and using the unstructured meshing library snappyHexMesh (sHM) in such a way that the mesh is refined in the vicinity of the floater to reduce computational cost.

The solver dynamicFvMesh is used to move the mesh surrounding the rigid body as it moves. Dynamic meshing is based on deformation of mesh without topological changes in the mesh configuration. The 2nd-order Newmark implicit solver is used for the time integration of the mesh motion. For mesh deformation, the spherical linear interpolation (SLERP) algorithm is used, in which mesh deformations (rotation and translation) are expressed using septentrions and quaternions. For each grid point, deformation is scaled from the full to no deformation based on the distance from the moving body surface. More information on dynamic meshing in OpenFOAM is provided by Jasak (2009).

Waves are generated and damped using the method described in (Jacobsen, Fuhrman and Fredsøe, 2012) by employing relaxation zones at inlet and outlet boundaries. Lateral boundaries are slip-free walls and the top wall has an atmospheric boundary condition. A preliminary test on the choice of turbulence modelling for the cases with fixed platform revealed no noticeable discrepancies between applying a turbulence model or running simulations in laminar mode (i.e., with no turbulence modelling) and using the molecular viscosity of water for dissipative terms. This was mainly due to the flow staying predominantly laminar in the cases considered. Therefore, to reduce the number of variables involved in the simulations and to save computational time, all cases presented here are computed using a laminar flow approach. This approach has also been practiced by (Petersen and Heilskov, 2015; Bruinsma, 2016; Rivera-Arreba, 2017) among others.

Variable time stepping is employed in all simulations by the Courant–Friedrichs–Lewy (CFL) number to ensure numerical stability and the 2nd order Crank-Nicolson scheme is used for the time integration of the fluid solver. The unbounded, conservative Gauss linear corrected scheme (second-order) is used for the Laplacian terms, while the gradient terms are discretised with linear Gaussian integration. The phase fraction equation is solved using a multi-dimensional universal limiter for explicit solution (MULES) algorithm, which ensures that values of scalar fields are bounded, e.g. in particular α remains between 0 and 1 (see Weller and Tabor, 1998). To relax the MULES limitation to Courant number, thereby reduce running

time, the semi-implicit version of MULES is applied to the current simulations, which first executes an implicit predictor step before constructing an explicit correction on which the MULES limiter is applied. Figure 1 shows a sketch of the numerical set up, numerical mesh and boundary conditions.

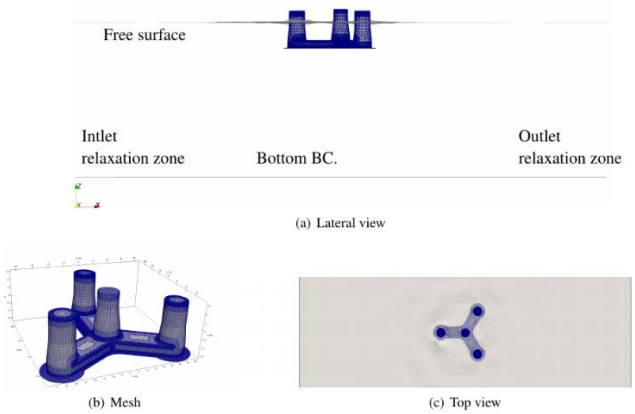

Figure 1: Schematic of the computational domain and boundary conditions

Results

Various kinds of simulations have been performed in order to characterise the hydrodynamic behaviour of the floater. First, a brief investigation of the excitation loads on the fixed platform for a range of regular waves are performed. The study continues with the dynamic behaviour of the free floater using heave decay tests. Finally, we examine the motion response of the free and moored floater to regular waves.

Table 1 summarizes the test parameters including type of the test, wave amplitude *a*, angular frequency ω, wave number, *k*, and water depth *h*. Figure 2 shows a snapshot of the floater in the CFD domain as it faces regular waves.

Table 1: Summary of the studied simulations.

Case	Type*	ω [rad/s]	a [m]	k [m^{-1}]	Wave type	h(m)
1-4	A	1	[0.5, 1.5, 2.5, 3.5]	0.11	Regular	130
5,6	B	ω_n	-	-	-	130
7,8	C	1	1	0.11	Regular	130

* **A**: fixed platform, **B**: Free heave decay at two different floater displacements, **C**: Floating body subject to waves with and without mooring.

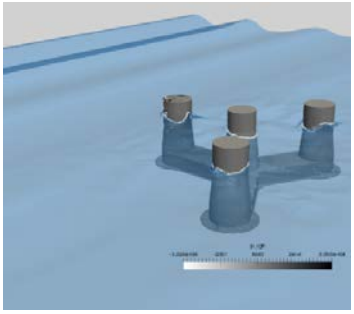

Figure 2: Snapshot of the OO-star floater in the numerical wave tank

Fixed platform

We investigate a fixed platform subject to waves of increasing height to examine the numerically predicted wave excitation loads. Regular waves of height 1 m to 3.5 m are used as specified in

Table 1. Figure 3 shows the results for vertical net force obtained with meshes of different "near-wall" and "base-mesh" refinement. Cases a), b) and f) each have a different base resolution (from fine to coarse) with the same sHM settings to examine the near wall refinement. Cases c), d), and e), on the other hand, all have the same base mesh as case b) but with different sHM settings. As can be seen, grids a) and c) give nearly identical predictions despite the large difference in the cell count. This suggests the importance of setting the right sHM parameters. The mesh using 0.75M cells is also shown to give results close enough to the more refined cases. For the following simulations mesh c) is used from the accuracy and computational cost perspectives.

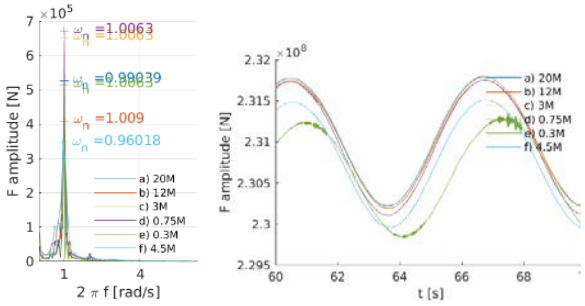

Figure 3: The sensitivity of forces on the fixed platform to the grid size

As mentioned in the previous section, the time step in the simulations is adjusted by the Courant–Friedrichs–Lewy (CFL) to ensure numerical stability. While a CFL number of less than unity is necessary to ensure numerical stability, a CFL number sensitivity is performed to examine the effect of the time step size. A range of CFL numbers from 0.1 to 1 is used to perform sensitivity studies similar to the mesh refinement and CFL = 0.15 is chosen for the current simulations based on the results as shown in Figure 4.

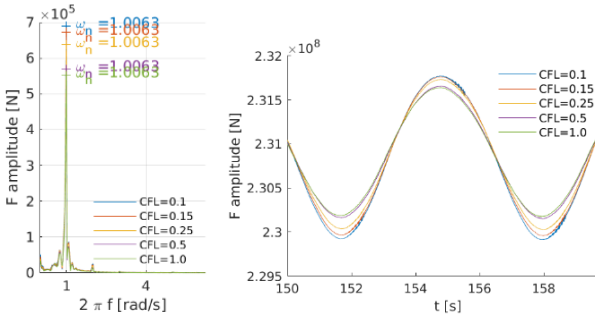

Figure 4: The sensitivity of forces on the platform to time step size through the CFL number

Figure 5 presents heave and surge force amplitude spectra of the fixed floater to waves of various steepness *ka*, where *k* and *a* are wave number and amplitude, respectively. The excitation peak frequency of the incoming waves is at $2\pi f = 1$, and higher harmonics are visible in all cases especially for the steeper waves.

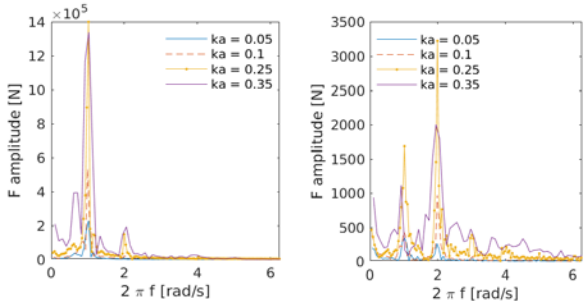

Figure 5: CFD results for wave excitation loads for the fixed platform in (left) heave and (right) surge.

Free decay tests

CFD simulations of the damped heave oscillatory motion are carried out to determine the decay response behavior of the un-moored floater in calm water. The results are compared to the FAST model of Pegalajar-Jurado, Madsen, *et al.*, (2018). To best reproduce the CFD setup, the FAST simulation was carried out with only the heave degree of freedom active, and with the mooring system disabled. In FAST, viscous effects are modelled with Morison drag. During the CFD simulations, it was found that the stability of the numerical solver has a strong sensitivity to the choice of released degrees of freedom, the numerical mesh and the floater mass. Among the tested setups, two simulations have been successfully running. In both cases, the degrees of freedom are limited to only heave. It was also observed that deactivation of the other-than-heave degrees of freedom improved the stability strongly. Figure 6 presents the resulting heave decay test.

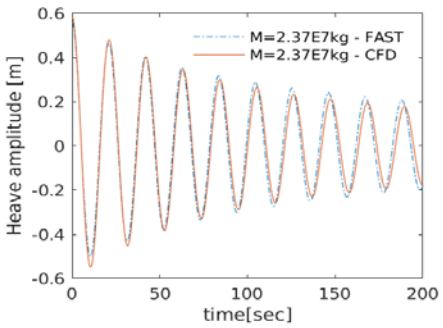

Figure 6: Free heave decay response: CFD vs. FAST simulations.

The average heave displacements are plotted against linear damping ratio in Figure 7 to assess the linearity of the damping effects. Four cases have been considered for comparison. In all cases the floater is only allowed to move in heave. Both CFD and FAST simulations are performed using M = 2.2709E7 kg and M = 2.3709E7 kg and without mooring restraints. From the figure, the linear damping ratio is seen to increase with amplitude, hence the damping is not just linear. It can also be realized that the level and trend of damping for FAST and CFD are comparable, with slightly higher damping level and slope observed for the CFD results.

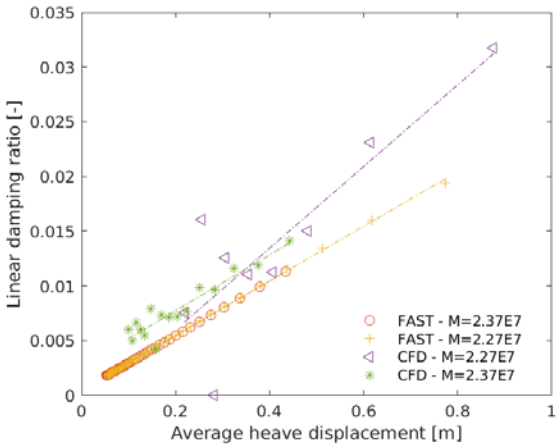

Figure 7: Identification of linear damping through decay tests: CFD vs. FAST simulations. All cases shown are non-moored.

Wave-induced motion of the OO-star platform

This section presents results of the floater motion and corresponding forces due to incoming waves. Two simulations with and without mooring are performed and a regular first order wave of steepness of ka = 0.1 is generated to excite the floater in heave motion. The excitation loads in time and frequency domain are shown in Figure 8. The two distinct peaks in the frequency plot refer to the wave frequency ($\omega_1 \approx 1$) and heave natural frequency of the floater ($\omega_2 \approx 0.3$). In order to take into account the mooring forces in the simplest realistic manner, the catenary mooring system is linearized using FAST (Pegalajar-Jurado, Madsen, *et al.*, 2018) and the stiffness values in the surge, heave and pitch degrees of freedom are applied on the centre of flotation. This is referred to as 'static mooring' in the figure. The heave forces shown in Figure 8 (top) qualitatively show how the mooring system contributes to limiting the heave excitation force. On the frequency domain, as seen from Figure 8 (bottom), the natural frequency will not noticeably change when the mooring is added since the heave stiffness (and hence natural frequency) is dominated by hydrostatics of the floater.

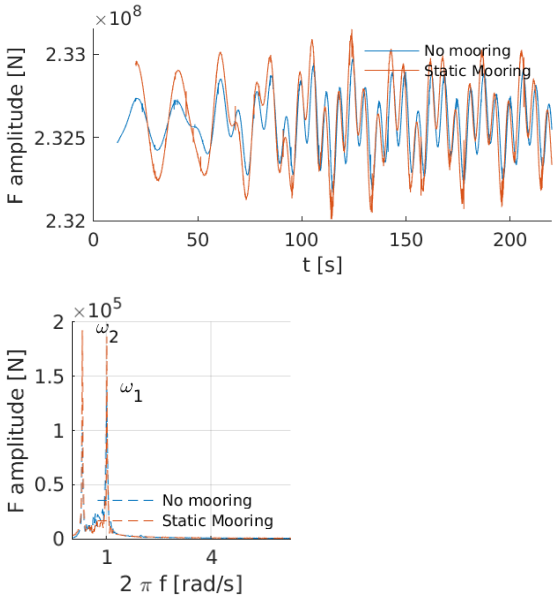

Figure 8: Heave force on the floater subject to incoming regular waves in (top) time domain, (bottom) frequency domain.

Concluding remarks

CFD simulations of the OO-star floater were conducted using the open source CFD toolbox, OpenFOAM. The floater geometry was modelled and an unstructured mesh was created using OpenFOAM's snappyHexMesh toolbox.

A mesh refinement study was conducted to guide the choice of mesh resolution and CFL number. Next, for a fixed platform, the heave excitation force was investigated with respect to wave amplitude and higher-harmonic force components were observed for increasing wave amplitude. Simulations of free heave decay were compared to FAST with a generally very good agreement for natural frequency, magnitude of damping and trend of increased damping for larger motion amplitude. Finally, the heave response to regular waves was compared for both a moored and a freely floating case. The results showed a clear reduction of the response due to the mooring system. While further investigation of the CFD set up is necessary, the results of this article suggest that CFD approaches may be used to predict complex flow phenomena in relation to floating offshore wind turbine platforms once a suitable numerical setup is established.

References

Benitz, M. A. *et al.* (2014) *Comparison of Hydrodynamic Load Predictions Between Engineering Models and Computational Fluid Dynamics for the OC4-DeepCwind Semi-Submersible: Preprint*.

Bredmose, H. *et al.* (2015) 'Experimental study of the DTU 10 MW wind turbine on a TLP floater in waves and wind', in *EWEA Offshore Conference, Copenhagen, Denmark, Mar*.

Bredmose, H. *et al.* (2017) 'The Triple Spar campaign: Model tests of a 10MW floating wind turbine with waves, wind and pitch control', *Energy Procedia*. Elsevier, 137, pp. 58–76.

Bruinsma, N. (2016) 'Validation and Application of a Fully Nonlinear Numerical Wave Tank', p. 144.

Dunbar, A. J., Craven, B. A. and Paterson, E. G. (2015) 'Development and validation of a tightly coupled CFD/6-DOF solver for simulating floating offshore wind turbine platforms', *Ocean Engineering*. Elsevier, 110, pp. 98–105. doi: 10.1016/j.oceaneng.2015.08.066.

Dunbar, A. J., Craven, B. A. and Paterson, E. G. (2015) 'Development and validation of a tightly coupled CFD/6-DOF solver for simulating floating offshore wind turbine platforms', *Ocean Engineering*. Elsevier, 110, pp. 98–105.

Jacobsen, N. G., Fuhrman, D. R. and Fredsøe, J. (2012) 'A wave generation toolbox for the open-source CFD library: OpenFoam®', *International Journal for Numerical Methods in Fluids*. Wiley Online Library, 70(9), pp. 1073–1088.

Jasak, H. (2009) 'Dynamic Mesh Handling in OpenFOAM', *47th AIAA Aerospace Sciences Meeting including The New Horizons Forum and Aerospace Exposition*, pp. 1–10. doi: 10.2514/6.2009-341.

Martin, H. R. *et al.* (2014) 'Methodology for wind/wave basin testing of floating offshore wind turbines', *Journal of Offshore Mechanics and Arctic Engineering*. American Society of Mechanical Engineers, 136(2), p. 20905.

Paulsen, B. T. *et al.* (2014a) 'Forcing of a bottom-mounted circular cylinder by steep regular water waves at finite depth', *Journal of Fluid Mechanics*, 755, pp. 1–34. doi: 10.1017/jfm.2014.386.

Paulsen, B. T. *et al.* (2014b) 'Forcing of a bottom-mounted circular cylinder by steep regular water waves at finite depth', *Journal of Fluid Mechanics*, 755, pp. 1–34. doi: 10.1017/jfm.2014.386.

Pegalajar-Jurado, A. *et al.* (2016) 'Experimental and numerical study of a 10MW TLP wind turbine in waves and wind', *Journal of Physics: Conference Series*, 753(9). doi: 10.1088/1742-6596/753/9/092007.

Pegalajar-Jurado, A., Madsen, F. J., *et al.* (2018) *LIFES50+ D4.5: State-of-the-art models for the two LIFES50+ 10MW floater concepts*.

Pegalajar-Jurado, A., Bredmose, H., *et al.* (2018) 'State-of-the-art model for the LIFES50+ OO-Star Wind Floater Semi 10MW floating wind turbine', *Journal of Physics: Conference Series*.

Petersen, O. S. and Heilskov, N. F. (2015) 'State-of-the-Art and Implementation of Design Tools for Floating Wave Energy Converters Part 2: Implementation and Results', (March). Available at: http://www.sdwed.civil.aau.dk/digitalAssets/103/103418_d1.5.pdf.

Rivera-Arreba, I. (2017) 'Computation of Nonlinear Wave Loads on Floating Structures', (July), p. 105.

Rusche, H. (2002) *Computational Fluid Dynamics of Dispersed Two-Phase Flows at High Phase Fractions*, *PhD Thesis*. Imerial College London. doi: 10.1145/1806799.1806850.

Sarlak, H., Seif, M. S. and Abbaspour, M. (2010) 'EXPERIMENTAL INVESTIGATION OF OFFSHORE WAVE BUOY PERFORMANCE', *Journal of Marine Engineering*, 6(11). Available at: http://www.ijmt.ir/browse.php?a_code=A-10-81-14&slc_lang=en&sid=1.

W. Yu, K. Müller, and F. L. (2018) 'LIFES50+ D4.2: Public Definition of the Two LIFES50+ 10MW Floater Concepts', pp. 1–105.

Weller, H. G. and Tabor, G. (1998) 'A tensorial approach to computational continuum mechanics using object-oriented techniques', *Computers in Physics*, 12(6), pp. 620–631. doi: 10.1063/1.168744.